Nat Hazards
https://doi.org/10.1007/s11069-018-3192-4

ORIGINAL PAPER

Hazard assessment of volcanic ballistic impacts at Mt Chihshin, Tatun Volcano Group, northern Taiwan

A. Nurmawati[1] · **K. I. Konstantinou**[1]

Received: 2 July 2017 / Accepted: 26 January 2018

Abstract This study investigates the hazard posed by Volcanic Ballistic Projectiles (VBPs) in the area surrounding Mt Chihshin, Tatun Volcano Group, northern Taiwan. Based on the volcano's current evolutionary stage, we consider two types of volcanic activity during which VBPs can be generated, namely hydrothermal and vulcanian eruptions. Hydrothermal eruptions may occur after a sudden decompression of water in the hydrothermal system of the volcano, typically due to mass removal processes, while vulcanian eruptions are caused by solidified magma that plugs the eruptive vent and gets blasted when this caprock is no longer able to withstand the pressure in the volcanic conduit. Initial velocities of ejected VBPs were estimated for each type of activity based on physical models and inserted as initial conditions to the equations that describe their motion. A hydrothermal eruption is assumed to occur at the NW flank of Mt Chihshin near the Hsiaoyiokeng fumarole, which is a place prone to flank instability, while a vulcanian eruption is assumed to originate from a central vent at the peak of Mt Chihshin. Modeling results suggest that the radii of the areas impacted by VBPs vary between 0.1 and 1.1 km for a hydrothermal eruption, while they become 1.4–5.1 km for a vulcanian eruption. Within these areas, roads, hiking trails, and public buildings lie within the impact areas; therefore, VBPs may potentially cause damage, injury, and even casualties.

Keywords Volcanic ballistic projectiles · Eruption · Volcanic hazard · Tatun · Taiwan

1 Introduction

Volcanic Ballistic Projectiles (VBPs) are particles with a diameter typically larger than 0.1 m that are produced by ejection of material during a vulcanian or hydrothermal eruption (Nairn and Self 1978; Yamagishi and Feebrey 1994; Michieli Vitturi et al. 2010). VBPs

✉ K. I. Konstantinou
kkonst@cc.ncu.edu.tw

[1] Department of Earth Sciences, National Central University, Jhongli 320, Taiwan, ROC

Published online: 05 February 2018

follow trajectories that may deviate from purely parabolic ones before they impact the ground. In terms of volcanic hazards, volcanologists have long been interested in studying the kinetic energies and landing temperatures of VBPs, since these particles may pose a threat to both people and buildings (Alatorre-Ibargüengoitia et al. 2012; Tsunematsu et al. 2014; Breard et al. 2014; Fitzgerald et al. 2014; Biass et al. 2016; Bertin 2017 among others). The hazards related to VBPs are a consequence of their high kinetic energy that allows them to penetrate even reinforced concrete, while their high impact temperature can cause fires especially if they fall within a vegetated area (e.g., Williams et al. 2017). It is for these reasons that hazard maps delineating the areas most likely to be hit by VBPs are considered an important tool for achieving risk mitigation.

The Tatun Volcano Group (herefter called TVG) lies just 15 km north from the city of Taipei, Taiwan, and consists of more than 20 volcanoes, the majority of which have erupted only once in the last hundred thousand years (Wang and Chen 1990; Song et al. 2000; Zellmer et al. 2015) (Fig. 1). Belousov et al. (2010) provide a comprehensive description of past volcanic activity at TVG; therefore, only a brief summary will be given

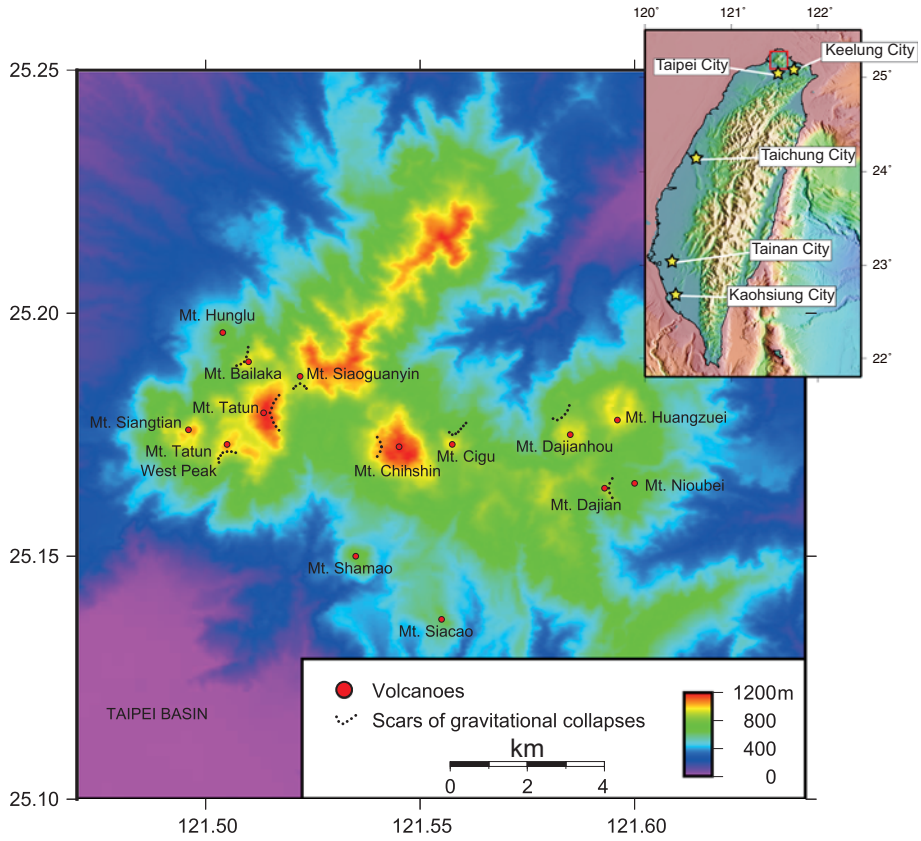

Fig. 1 Map showing the area covered by the different volcanic edifices of the Tatun Volcano Group. The scar traces of past gravitational collapses have been adopted from Belousov et al. (2010). The limits of Taipei City roughly coincide with the limits of the Taipei Basin. The inset at the upper right-hand corner shows the location of TVG (marked with a red square) on the map of Taiwan and the locations of major cities

here. In the last 23,000 years, volcanic activity at TVG ranged from voluminous effusion of crystal-rich lava to weak phreatic and highly explosive Plinian eruptions. However, vulcanian explosions were also very common, as judged by the presence in the area of dense ballistic blocks and lithic ashes. The last volcanic activity at TVG occurred about 6000 years ago and involved a series of small-scale phreatic explosions near Mt Chihshin, which is the most well-preserved edifice of all TVG volcanoes. Geophysical as well as geochemical observations suggest that TVG is a presently dormant but still active volcanic group, and therefore an eruption may occur in the future (Yang et al. 1999; Konstantinou et al. 2007; Rontogianni et al. 2012; Zellmer et al. 2015; Lin 2016 and references therein). For this reason, TVG is closely monitored by a number of seismic and GPS stations operated by the Tatun Volcano Observatory (TVO). Fumarolic activity is also very strong at several sites in the TVG area with the Hsiaoyiokeng fumarole, at the NW flank of Mt Chihshin, being situated along a gravitational collapse scar. This previous history of vulcanian and phreatic eruptions suggest that VBPs represent an important hazard at TVG. Despite this, no work has been done previously in order to model and assess the hazard posed on buildings, as well as on the thousands of people visiting TVG for recreation purposes every year.

In this work, we present a first-order hazard assessment of the spatial extent of areas around Mt Chihshin that may be affected by the impact of VBPs ejected by two hypothetical eruptions, one hydrothermal and another vulcanian. First, we give a description of the ballistic equations that will be used for calculating trajectories, impact velocities, and maximum horizontal distances of individual VBPs. Initial ejection velocities are then estimated for two different scenarios, one involving a sudden decompression of the hydrothermal system and the other assuming a solidified caprock that is blasted during a vulcanian-type explosive eruption. Based on these initial conditions and the ballistic model, impact points and landing kinetic energies of VBPs are estimated for the purpose of delineating hazard zones around Mt Chihshin. Finally, we close with the main conclusions regarding the risk posed by VBPs in this area and suggestions for future work.

2 Ballistic model

The equations that describe the motion of VBPs from their ejection point to the point they impact the Earth's surface are derived by using Newton's second law and by considering that gravity as well as drag forces is applied to each particle (for an overview, see Taddeucci et al. 2017; Bertin 2017). Following Mastin (2001) and Alatorre-Ibargüengoitia et al. (2012) in this study, the VBP motion is considered as two-dimensional and its acceleration along a horizontal (x) and the vertical (z) axis is described by a system of ordinary differential equations as

$$\frac{\mathrm{d}v_x}{\mathrm{d}t} = -\frac{AC_\mathrm{d}\rho_\mathrm{a}(z)(v_x - u_x)|v-u|}{2m} \tag{1}$$

$$\frac{\mathrm{d}v_z}{\mathrm{d}t} = -\frac{AC_\mathrm{d}\rho_\mathrm{a}(z)v_z|v-u|}{2m} - g \tag{2}$$

where v_x and v_z are the velocities of the VBP in each direction and $\mathbf{v} = (v_x, v_z)$ represents the velocity vector, t is time, A and m are the cross-sectional area and mass of the VBP respectively, C_d is the drag coefficient, $\rho_\mathrm{a}(z)$ is the air density for a given altitude z,

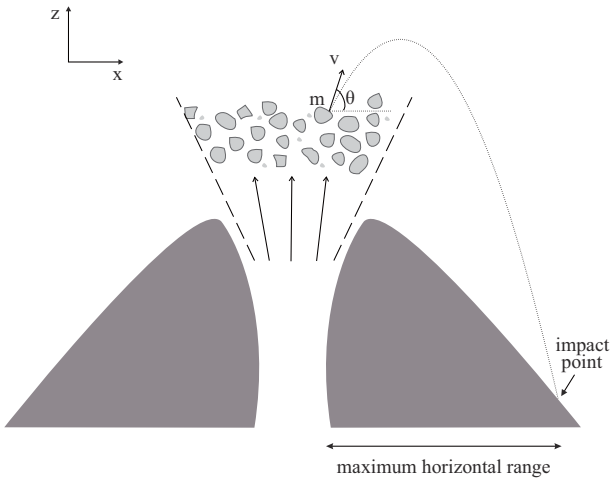

Fig. 2 Cartoon illustrating the main physical parameters involved in the calculations of ballistic trajectories for VBPs. A VBP with mass m is ejected at an angle θ with initial velocity v and follows a quasi-parabolic trajectory before it impacts the Earth's surface. The maximum horizontal distance traveled by the VBP is then defined as the distance from the ejection point to the point of impact

Table 1 Parameter values utilized for the calculation of air density as a function of elevation

Quantity	Value
p_0	10^5 Pa
T_0	288 K
g	9.81 m/s^2
M_a	0.028964 kg/mol
Λ	0.0065 K/m
R	8.314J/(mol K)

$\mathbf{u} = (u_x, 0)$ is the wind velocity, and g is the acceleration of gravity. The expression $|v - u|$ describes the effect of wind velocity on the VBP velocity and in this case, is given by

$$|v - u| = \sqrt{(v_x - u_x)^2 + v_z^2} \tag{3}$$

Usually, the cross-sectional area and mass of the VBP are not known; therefore, in the case of a spherical projectile, it is convenient to substitute A/m with the quantity $3/(2\rho_b D)$, which involves the VBP density ρ_b and its diameter D. VBPs are assumed to leave the ejection point at an angle θ, and this implies that the velocities in the x and z directions will be $v\cos\theta$ and $v\sin\theta$, respectively (Fig. 2).

The ballistic model should also take into account the change of air density as a function of altitude z. This means that at each integration step, the air density has to be recalculated by assuming that the air is a perfect gas and that the pressure is given by the following equation (Mastin 2001)

$$p(z) = p_0\left(1 - \frac{\Lambda z}{T_0}\right)^{\frac{gM_a}{R\Lambda}}, \tag{4}$$

where p_0 and T_0 are the pressure and temperature at sea level, R is the ideal gas constant, M_a is the molar mass of dry air, and Λ is the thermal lapse rate. Table 1 summarizes the

values of these parameters that have been adopted for all subsequent calculations. Using these calculated pressure values, it is then possible to obtain air density by utilizing the relationship $\rho_a(z) = p(z)M_a/RT_0$.

The drag coefficient (C_d) is a dimensionless quantity that is equal to the ratio of the drag force divided by the product of kinetic energy and the cross-sectional area of the VBP. Experimental observations show that the drag coefficient depends on both the Reynolds and Mach numbers (Mastin 2001; Alatorre-Ibargüengoitia and Delgado-Granados 2006; Bertin 2017; Taddeucci et al. 2017). The former number gives a measure of the relative importance of viscous over inertial forces and may fluctuate significantly around a critical value that signifies the transition from laminar to turbulent boundary layer (also known as 'drag crisis' see Bertin 2017). The latter represents the influence that compression of the fluid has on the flow of air around a VBP. As it can be seen in Fig. 3, the value of the drag coefficient for different geometrical shapes (sphere or cube) exhibits sharp changes around Mach 1 maintaining an almost constant value after Mach 3. Due to the lack of experimentally determined drag coefficients for VBPs specifically at TVG and for the sake of simplicity, we assume a constant drag coefficient of 0.65 when the Mach number is less than 0.5, while for larger Mach numbers, we use drag coefficient values corresponding to a low cube. The velocity v of the VBP is divided by the sound speed of the air c in order to calculate the Mach number at each integration step, and the appropriate drag coefficient is then adopted from tabulated values of the curve shown in Fig. 3.

Visual observations suggest that once ejected from the vent, VBPs quickly become enveloped by an expanding mixture of gas and fine particles that move at roughly the same velocity as the VBPs (Fagents and Wilson 1993; Michieli Vitturi et al. 2010). This phenomenon has typically been modeled by means of a reduced drag coefficient over some distance away from the vent (Fagents and Wilson 1993; Mastin 2001). In order to incorporate this effect into our calculations, we assume that after ejection the VBP moves within a reduced drag zone of radius r_d, which is a function of radial distance r from the ejection point. In this case, Mastin (2001) approximates the reduced drag coefficient C_{dr} as

$$C_{dr} = C_d\left(\frac{r}{r_d}\right)^2 \tag{5}$$

Based on empirical observations and theoretical considerations, the value of r_d should range from tens to hundreds of meters (Nairn and Self 1978; Mastin 2001); therefore, in our calculations, we will effectively treat it as a free parameter.

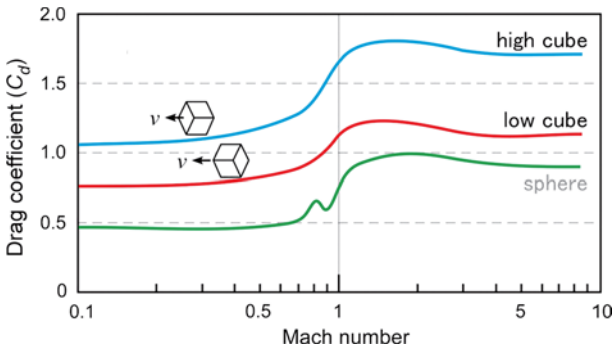

Fig. 3 Diagram showing the variation in the drag coefficient C_d as a function of the Mach number. The three curves describe experimentally determined drag coefficients for different shapes (sphere or cube) and orientation (cube facing the flow with its edge, or its side) (from Maeno et al. 2013)

In order to solve Eqs. (1) and (2), initial conditions in the form of launch height and velocity of VBPs are needed; however, these quantities depend on the type of eruption and where this eruption will originate. In our simulations, we consider two hypothetical scenarios of a hydrothermal and a vulcanian eruption occurring at Mt Chihshin. The chosen site of the hydrothermal eruption is the Hsiaoyiokeng fumarole, not only because an eruption there can potentially cause numerous injuries/casualties (the fumarole is easily accessible to visitors), but also because the NW flank of Mt Chihshin is prone to gravitational collapses which could trigger such an eruption (cf. Fig. 1). Belousov et al. (2010) also note that Mt Chihshin can be considered as a polygenetic cone that is structurally transitional to a stratovolcano, so the most likely eruptions during its current evolutionary stage will be vulcanian. It is therefore reasonable to place the site of the vulcanian eruption at the peak of Mt Chihshin.

3 Initial conditions for VBP ejection

3.1 Hydrothermal eruption

A hydrothermal eruption may occur after a sudden decompression, when the water that exists in the surface layers of a volcano edifice reaches temperatures of up to 250 °C and flashes to steam, blasting the confining rocks and ejecting within a radius of tens to hundreds of meters solid material along with steam and liquid water (Muffler et al. 1971; Mastin 1995). The energy of a hydrothermal eruption is derived solely from the hot expanding steam, while magma is passively involved in the process by providing the necessary heat. Even if extra heat is added to the system, it may still not cause immediate water boiling and steam production, for the reason that the lithostatic pressure may increase the boiling temperature. Mass removal processes, for instance in the form of a landslide, can cause a sudden lithostatic pressure drop exposing the high temperature mixture of water and rock to atmospheric conditions that result in its explosive expansion.

The fraction of water X that will be vaporized when that mixture of water and rock expands isothermally to its final state can be calculated as (Muffler et al. 1971)

$$X = \frac{m_{\mathrm{w}} c_{\mathrm{w}} \Delta T + m_{\mathrm{r}} c_{\mathrm{r}} \Delta T}{m_w L}, \tag{6}$$

where m_{w} and m_{r} are the masses of water and rock, respectively, c_{w} and c_{r} are their specific heat values, L is the heat of vaporization for water, and ΔT is the temperature difference between the initial state and final state of the system. The thermal energy ΔE_{th} available for breaking the rock and creating a crater, as well as uplifting the material, can be calculated if we take into account the transfer of energy between internal energy U and other forms of energy (such as seismic energy). Based on thermodynamic considerations, Muffler et al. (1971) suggested that this energy can be given by

$$\Delta E_{th} = m_{\mathrm{r}} c_{\mathrm{r}} \Delta T + X m_{\mathrm{w}} (U_{\mathrm{w},i} - U_{s,f}) + (1 - X) m_{\mathrm{w}} (U_{\mathrm{w},i} - U_{\mathrm{w},f}), \tag{7}$$

where $U_{w,i}$ and $U_{w,f}$ are the internal energy of water at its initial state and final state, respectively, while $U_{s,f}$ is the internal energy of steam at its final state. The kinetic energy E_k that the ejected material will attain is only a fraction η of ΔE_{th}, which means that (see Montanaro et al. 2016)

$$E_k = \eta \Delta E_{th}, \tag{8}$$

where η represents the conversion coefficient from one form of energy to another. Recently, Montanaro et al. (2016) studied the energy budget of a hydrothermal eruption at Gengissig lake (Kverkfjöll volcano) in Iceland, determining η to be in the range of 0.08–0.12. This range will be also used in this study during subsequent calculations. The velocity v of the ejected material can then be estimated as

$$v = \sqrt{\frac{2\eta \Delta E_{th}}{m_{\mathrm{r}}}} \tag{9}$$

Before estimating v, we have to calculate the thermal energy ΔE_{th} involved in the process. In order to do this, we need to define the initial state and final state of the system in terms of internal energy and temperature difference, as well as to calculate the rock mass m_{r} and water mass m_{w}. Prior to the hydrothermal eruption, water is assumed to be under a lithostatic pressure of 0.49 MPa (which corresponds to a depth of 20–50 m) and has an initial temperature that varies between 118 and 218 °C. After the mass removal, the rock and water mixture is assumed to be exposed to an atmospheric pressure of 0.092 MPa that is compatible with an elevation of 900 m (elevation of the Hsiaoyiokeng fumarole), where the boiling temperature of water is 98 °C. Since hydrothermal eruptions produce large size craters, rock mass is calculated from the empirical relationship $D = 0.9V^{0.36}$ (Sato and Taniguchi 1997), where D is the crater diameter and V is the volume of excavated rock. This relationship was derived for phreatomagmatic eruptions; however, such eruptions can be considered as the most similar to hydrothermal ones. A crater diameter of 170 m is chosen here for the reason that this value corresponds to the largest crater formed after hydrothermal eruptions at Mt Chihshin (Belousov et al. 2010). The volume of rock obtained is 1.7×10^6 m^3, which can be converted into mass by assuming a specific rock density. On the other hand, water mass can be easily calculated as $m_{\mathrm{w}} = \phi \rho_{\mathrm{w}} V$, where ϕ is rock porosity and ρ_{w} is water density at a pressure of 0.49 MPa. Internal energies U of water and steam at particular temperatures were obtained from thermodynamic tables (Cengel and Boles 2002), while the heat needed to vaporize water was taken as $L = 2.276\times10^6$ J/kg.

The temperature difference ΔT before and after the hydrothermal eruption strongly influences the obtained velocity of the ejected material. Figure 4a shows the variation in ejection velocity as a function of ΔT if rock density is taken as 1100 kg/m^3 and a value of 0.3 is assumed for rock porosity. It can be seen that for $\eta = 0.12$, ejection velocity attains a maximum of 50 m/s at ΔT = 100–120 °C, while for $\eta = 0.08$, this maximum becomes 40 m/s. On the other hand, keeping a constant value of ΔT equal to 120° C, and varying the rock density from 1100 to 2300 kg/m^3 and porosity between 0.1 and 0.5, produces only small changes in velocity (< 10 m/s) (Fig. 4b, c). In subsequent calculations, we will utilize the velocity of 50 m/s as the initial velocity of VBPs during the hydrothermal eruption.

3.2 Vulcanian eruption

Vulcanian eruptions occur when magma extrudes and solidifies at the top of a vent forming a caprock which then plugs the eruptive vent (Parfitt and Wilson 2008). As the vent is plugged, the pressure in the conduit keeps increasing and when the caprock is no longer able to withstand the pressure, an explosion occurs and the caprock is ejected. Alatorre-Ibargüengoitia et al. (2010) developed a laboratory model for vulcanian eruptions by considering that the total energy during such an eruption is divided into energy used for rock fragmentation and the energy used for ejecting the material. In this model, the pressure available for ejecting the

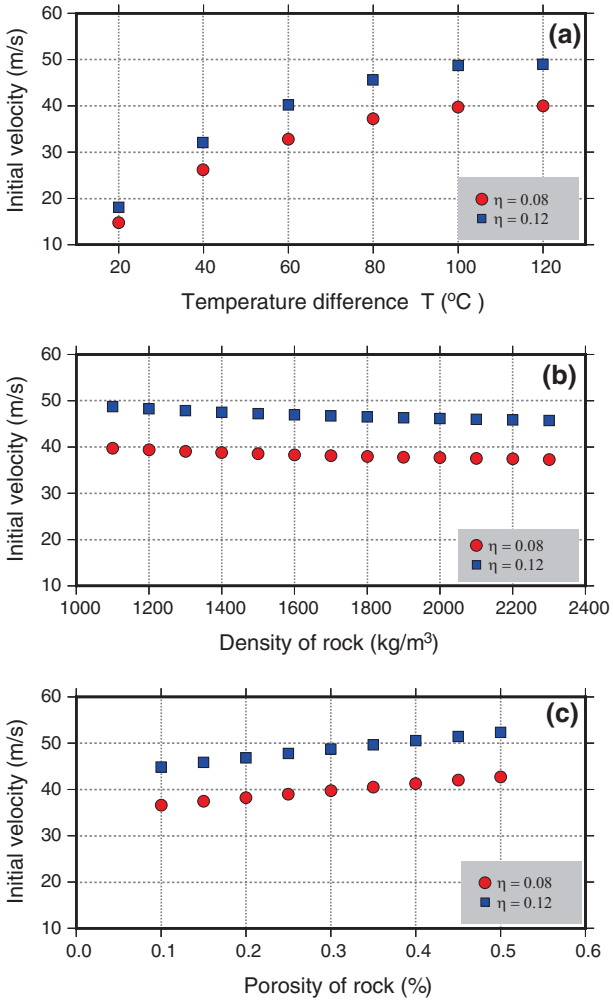

Fig. 4 Diagrams showing the variation in initial velocity of a VBP ejected during a hydrothermal eruption as a function of **a** the temperature difference ΔT assuming that rock density is 1100 kg/m^3 and porosity 0.3, **b** rock density assuming that $\Delta T = 120°$ C and porosity 0.3, and **c** rock porosity assuming that $\Delta T = 120°$ C and rock density is 1100 kg/m^3. Two sets of values are shown corresponding to different energy conversion coefficient η (see text for more details)

material is $P_{ef} = P_0 - P_{th}$, where P_0 is the initial gas pressure in the volcanic conduit and P_{th} is the fragmentation pressure threshold of magma, which is defined as the minimum pressure required to completely fragment the caprock (Spieler et al. 2004). Utilizing laboratory observations, Alatorre-Ibargüengoitia et al. (2010) derived an ordinary differential equation that can be used to calculate the velocity v_c of the ejected caprock during a vulcanian eruption, which is

$$\frac{dv_c}{dt} = \frac{A_c}{m_c}\left\{P_{ef}\left[1 - \frac{1}{2}(\gamma - 1)\frac{v_c}{\sqrt{n\gamma RT_0}}\right]^{\frac{2\gamma}{\gamma-1}} - P_{ext}\right\} - g \tag{10}$$

where v_c is caprock velocity, m_c and A_c are mass and cross-sectional area of the caprock, respectively, γ is the specific heat capacity ratio, n is the mass fraction of gas, R is the ideal gas constant, T_0 is the initial temperature, and P_{ext} is the atmospheric pressure above the caprock ($\sim 10^5$ Pa). The main gas phase involved in propelling the caprock is considered to be water vapor with $\gamma = 1.27$ and $R = 462\,\mathrm{J/kg/K}$ at a temperature $T_0 = 1123$ K (Alatorre-Ibargüengoitia et al. 2010). The ratio A_c/m_c can be substituted by $1/\rho_c H_c$, where ρ_c is the density of the caprock and H_c is its thickness assuming that it can be modeled as a cylinder. The density of the caprock is taken equal to $1900\,\mathrm{kg/m^3}$, which is consistent with density measurements of rocks from Mt Chihshin (Belousov et al. 2010). The thickness of the caprock is assumed to be 15 m, taking into account that variation of this parameter from 15 to 25 m causes a reduction in caprock velocity by about 10–15%.

Equation (10) was numerically solved using the implicit Runge–Kutta method (e.g., Hairer and Wanner 2010) for the time interval of 0–3 s, which is the time when the caprock can be considered as one block before it disintegrates (Alatorre-Ibargüengoitia et al. 2010). Here, we chose initial gas pressure P_0 to vary up to 25 MPa for the reason that this value represents the upper limit of overpressure inside conduits at several volcanoes (e.g., Alatorre-Ibargüengoitia et al. 2010; Burgisser et al. 2011). Spieler et al. (2004) give a range of P_{th} values between 2 and 20 MPa for rocks at different volcanoes around the world. Larger values of fragmentation pressure threshold will tend to significantly lower the caprock velocities, as less pressure will be available for the ejection of VBPs. Since there are no P_{th} data for Mt Chihshin, and because we are interested in establishing the maximum distances that VBPs can attain, we adopt here the lowest P_{th} value (2 MPa). Figure 5 shows the variation in caprock velocity as a function of initial pressure for gas mass fraction equal to 0.01 and 0.06; larger fractions of gas mass produce unrealistically large (> 500 m/s) caprock velocities. In the case of $n = 0.01$, the caprock velocity tends to attain a maximum value of $190\,\mathrm{m/s}$($M = 0.5$), while for $n = 0.06$, the velocity becomes $370\,\mathrm{m/s}$ (slightly above sound speed with $M = 1.2$). Consequently, we will utilize the latter velocity value in order to find the maximum distance of VBPs at Mt Chihshin.

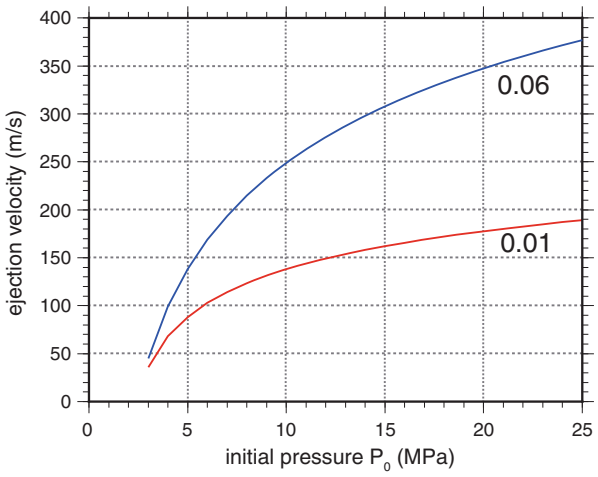

Fig. 5 Variation in caprock ejection velocity versus initial pressure P_0 for fragmentation threshold pressure of 2 MPa. The two curves shown represent the two different gas fractions used (0.01 and 0.06)

4 Results

4.1 Delineation of impact areas

For each eruption scenario considered in this study, the system of ordinary differential equations describing the VBP motion was numerically solved by using the implicit Runge–Kutta method and the corresponding initial velocities. The VBPs during the hydrothermal eruption are assumed to be ejected at a site near the Hsiaoyiokeng fumarole, which is located at an elevation of 900 m at the NW flank of Mt Chihshin. On the other hand, the ejection point of the caprock for the vulcanian eruption is assumed to be the peak of Mt Chihshin ($\sim$ 1100 m) and this choice implies a central vent eruption, which is the most likely scenario. Simulations were conducted by considering three VBP diameters, namely 0.2, 1.0, and 2.0 m. We note that the diameter of 2 m is slightly larger than the largest VBP ($\sim$ 1.5 m) reported around Mt Chihshin by Belousov et al. (2010). Ejection angle was varied between 20° and 70° in order to find the optimal range that maximizes the horizontal distance. VBP density was set to 1900 $\mathrm{kg/m^3}$ according to the measurements of Belousov et al. (2010). As stated earlier, the reduced drag radius is considered as a free parameter and four values were assumed, namely 100, 200, 300, and 400 m. A tailwind velocity of 20 m/s was also included in the calculations since this part of northern Taiwan is prone to strong winds that might affect the horizontal trajectory of VBPs. Even though we considered the influence of topography on the horizontal distances, the available digital elevation model (DEM) of Taiwan has a rather coarse resolution of 40 meters. We therefore opted for presenting the hazard zones on the map as radii of maximum horizontal extent without showing how these would distort due to the topography. Table 2 summarizes the range of optimal ejection angles and maximum horizontal distance traveled by VBPs for each scenario considered.

Based on the model previously outlined in Sect. 3.1, we set the initial velocity of VBPs to 50 m/s assuming that the energy conversion coefficient takes its largest value ($\sim$ 0.12). The hazard zones at elevations higher/lower than the site of the hydrothermal eruption are shown in Fig. 6. It should be noted that locations at higher elevation may be impacted by VBPs as well; however, the ejection angle of these VBPs has to be larger than the dip of the slope uphill 40°–50°. This has the consequence that the range of the VBPs will be smaller than that reached when the ejection angle is within the optimum range. At lower elevations, the maximum horizontal distance traveled never exceeded 0.3 km with optimal ejection angles between 30° and 50°, while at higher elevations and ejection angles larger than 50°, this range became 0.1 km. However, it is also possible that the initial velocity of VBPs may exceed our estimate of 50 m/s. Indeed, Browne and Lawless (2001) compiled a catalog of hydrothermal eruptions worldwide and they report a few occurrences where VBP initial velocities reached values of 200 m/s. For the purpose of investigating the effect

Table 2 Summary of optimal ballistic parameters for the different scenarios considered in this study

v_{in}	θ	$d_{\max}$ (0.2 m)	d_{max} (1.0 m)	d_{max} (2.0 m)	Type
50 m/s	30°–50°	0.24 km	0.28 km	0.3 km	Hydrothermal
200 m/s	30°–50°	0.41 km	0.83 km	1.1 km	Hydrothermal
370 m/s	20°–50°	5.1 km	1.8 km	1.4 km	Vulcanian

v_{in} symbolizes the initial velocity of the VBP, θ its ejection angle, and $d_{\max}$ the maximum distance of each diameter VBP (0.2, 1.0, 2.0 m) within this range of θ

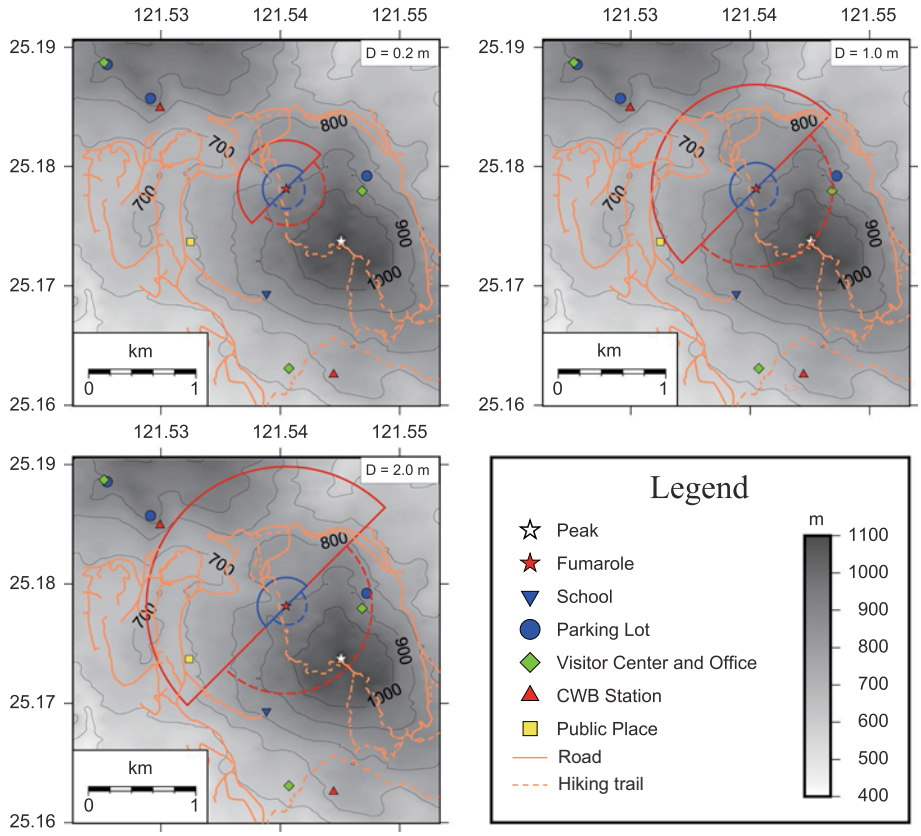

Fig. 6 Delineation of impact areas for three VBP diameters ejected during the scenario of a hydrothermal eruption at the Hsiaoyiokeng fumarole. At lower elevation, the solid blue line corresponds to the maximum distance traveled by a VBP with initial velocity of 50 m/s and the solid red line with an initial velocity of 200 m/s. At higher elevation, the dashed blue line represents the maximum distance traveled by VBPs that are ejected at angles larger than 50° with initial velocity of 50 m/s. The dashed red line represents maximum distance traveled by VBPs at angles larger than 50° with initial velocity 200 m/s

of a higher initial velocity on the distance traveled by the VBPs, we ran a new set of simulations. The results show that the larger diameter VBPs (1.0, 2.0 m) could reach horizontal distances of 0.9–1.1 km for the optimal ejection angles at lower elevation. At higher elevation, these distances do not exceed 0.7 km for ejection angles larger than 50°. Maximum vertical extent for all three diameter VBPs was found between 0.9 and 0.95 km asl. In the lower elevation areas that may be affected by VBPs, there are no buildings; however, there are public roads/hiking trails and a botanical garden. At higher elevation, except from roads and hiking trails, the visitor center and its parking lot may be impacted by VBPs. Considering that hydrothermal eruptions may occur without much warning, the potential for serious injury and/or casualties is high since these areas represent a favorite place of recreation for tens of thousands of people, especially during the weekends or public holidays.

The scenario concerning a vulcanian eruption at Mt Chihshin involves a larger horizontal and vertical maximum extent that VBPs may travel. In this scenario, the smallest diameter VBP is the one that reaches the largest horizontal distance (~5.1 km), while the

VBPs with diameters of 1.0 and 2.0 m reach distances of 1.8 and 1.4 km, respectively, for optimal ejection angles 20°–50° (Fig. 7 and Table 2). Most of the buildings situated within the impact area of VBPs are public buildings such as the national park visitor centers and their corresponding parking lots, but also the Hutian Elementary School and the campus of the Chinese Culture University. Another aspect that must be considered during a vulcanian eruption is the threat posed to aircraft when VBPs reach maximum vertical height. According to the Civil Aeronautics Administration of Taiwan (http://www.caa.gov.tw, last accessed 25 September 2017), the height of an airplane above Mt Chihshin as it is performing its landing approach to Taipei's Songshan Airport is approximately 1.5 km above ground or 2.4 km asl. Our simulations show that the maximum height of VBPs during vulcanian eruptions may also reach 2.4 km asl, suggesting that VBPs can also be a threat to approaching aircraft. As an overview of all these scenarios, Fig. 8 shows maximum horizontal distance that VBPs of different sizes can reach if ejected at the aforementioned velocities and an optimal angle of 40°, where it is obvious that VBPs smaller than 1.0 m in diameter will attain larger horizontal distance.

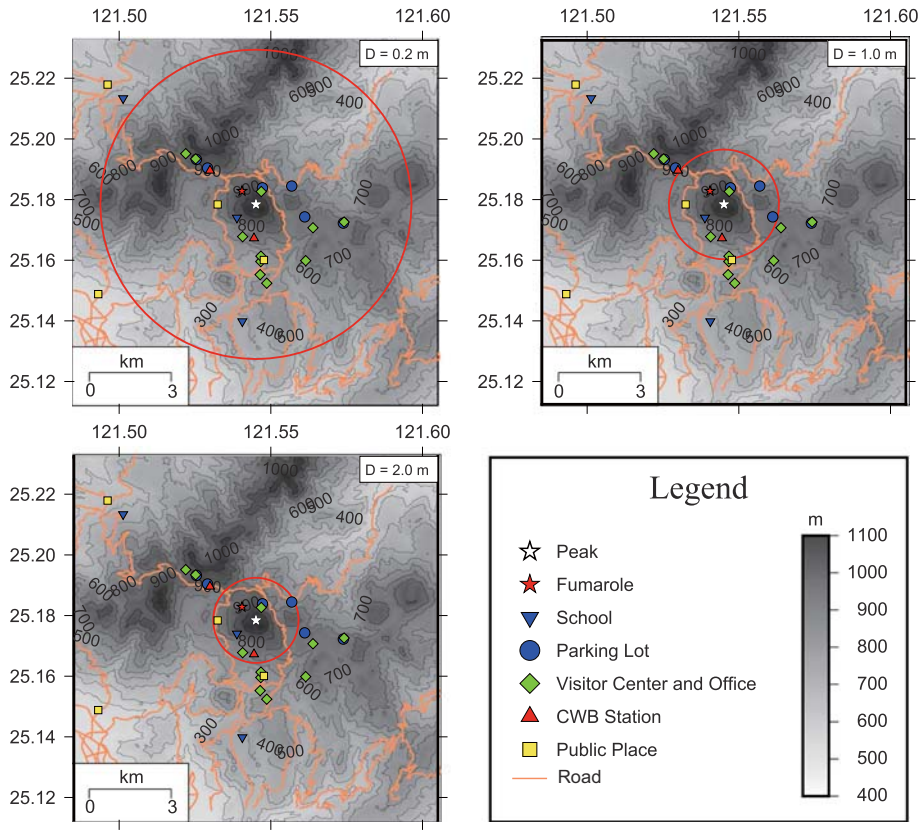

Fig. 7 Same as in Fig. 6 for the scenario of a vulcanian eruption originating at the peak of Mt Chihshin

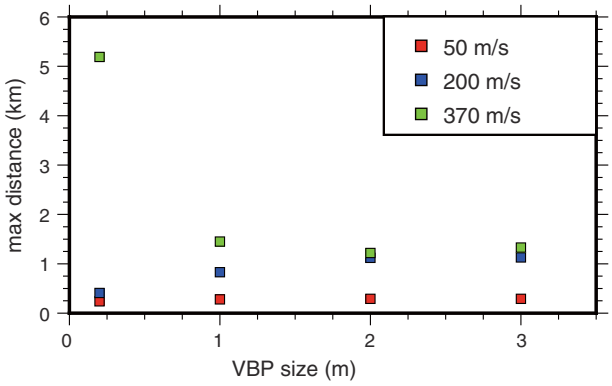

Fig. 8 Diagram showing the variation in maximum horizontal distance a VBP can travel as a function of its size. Three different ejection velocities are considered and the VBPs are assumed to eject at an angle of 40° within a reduced drag zone of 200–400 m radius

4.2 Assessment of damage to buildings

The numerical solution of the ballistics equations also provides for every simulation the landing velocity of each VBP at its point of impact. The kinetic energy at the impact site can then be calculated in order to check the structural vulnerability of buildings to VBPs. Spence et al. (2005) investigated the relationship between impact kinetic energy and damage caused to several different building materials such as glass, fiber cement, plywood, steel sheets, and reinforced concrete (RC) slabs. Considering that in the vulcanian eruption scenario several buildings were within the impact areas, the results of Spence et al. (2005) have been adopted in this study and plotted on a diagram along with the average impact kinetic energy for each diameter VBP (Fig. 9). We observe that VBPs of 0.2 m diameter can penetrate all materials except perhaps from RC slabs whose strength range may be a bit higher than the VBP impact kinetic energy. On the other hand, VBPs with larger diameters are able to penetrate all of the building materials considered here. The school and visitor center buildings that may be impacted by VBPs at TVG are made of RC slabs but also incorporate glass in their exterior facade. More importantly, the roofs of these buildings are covered by ceramic tiles whose strength is likely much less than RC slabs. However,

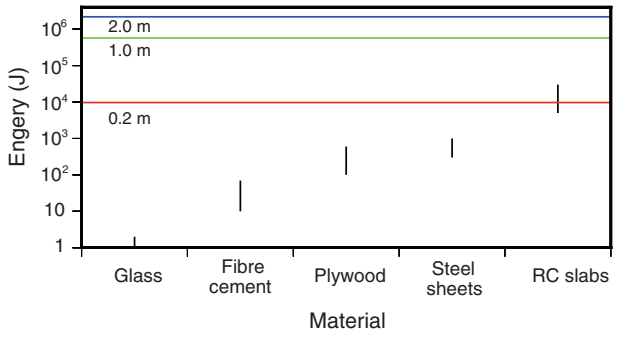

Fig. 9 Kinetic energy versus strength for five different building materials adopted from Spence et al. (2005). Horizontal lines indicate impact kinetic energies for three VBP diameters ejected during a vulcanian eruption, while vertical lines represent the range of kinetic energies that building materials can withstand without being penetrated

in a recent study, Williams et al. (2017) showed that VBP-related damage also depends on whether the VBP will hit the building in a perpendicular direction or obliquely. In the former case, the probability of penetration increases significantly, while in the latter one, the VBP may only cause damage to the exterior of the building. We can therefore conclude that while the buildings at TVG are vulnerable to VBP impacts of all diameters, it is likely that only a fraction of these impacts can be dangerous for the people inside these buildings.

5 Conclusions

Ejection of VBPs during explosive volcanic eruptions is a common phenomenon and is also the one posing serious hazards. The main conclusions of this study regarding the areas of VBP impact at TVG and recommendations for risk mitigation can be summarized as follows:

1. VBPs produced by a hydrothermal eruption at the Hsiaoyiokeng fumarole may travel to a maximum horizontal distance of a few hundred meters (0.3–1.1 km) at lower elevation when ejected at optimum angles. Within these radii, there are roads and hiking trails but no buildings. At higher elevations, the distance range becomes 0.1–0.7 km due to the increase in the ejection angles to values larger than 50°. In this case, the visitor center and its parking lot lie within the impact area, as well as the hiking trail that leads to the top of Mt Chihshin. VBPs and the explosion blast wave may therefore cause serious injury to the visitors / hikers that may happen to be nearby at the time of the eruption. One way to mitigate that risk would be to restrict access to visitors within the aforementioned radii around the Hsiaoyiokeng fumarole.
2. The impact distances of VBPs during a vulcanian eruption originating at the peak of Mt Chihshin could range from 1.4 to 5.1 km depending on the size of VBPs. Several buildings (visitor centers, schools) and public places (parking lots, botanical garden) are within the range of VBPs, and their impact might potentially cause serious damage and injuries. If the vulcanian eruption occurs without much warning, then aircraft approaching Taipei's Songshan Airport from the North, flying at an altitude of about 2.4 km asl, is also in danger of being hit by VBPs.
3. During a vulcanian eruption, VBPs can attain kinetic energy levels high enough to penetrate the materials that most buildings at TVG (schools, visitor centers) are made of (RC slabs, glass, ceramic tiles). However, VBPs that will hit the buildings obliquely are unlikely to penetrate them; therefore, the people inside may enjoy some level of protection. Retrofitting the roofs of the buildings at TVG with extra layers of material (timber or metal sheets) may effectively inhibit inward penetration from occurring by reducing the impact velocity of VBPs (Williams et al. 2017).

VBPs impact is one of many volcanic hazards (others being pyroclastic flows, lahars, etc) that may threaten the area around Mt Chihshin (see also Konstantinou 2015). More research into their probabilities of occurrence and their effects is needed in order to propose more specific recommendations to the authorities. The results presented in this study can be further enhanced by determining more accurate values for some of the parameters involved in the ballistic and caprock models. Drag coefficients could be experimentally determined for VBPs sampled from Mt Chihshin and its surroundings. In this way, assumptions about the VBPs shape and the value of the drag coefficient for different Mach numbers would be

avoided. Fragmentation pressure threshold for TVG rocks could in a similar way be determined experimentally and constrain the ejection velocity of the caprock during a vulcanian eruption. A map of preserved VBPs from previous eruptions could also give valuable information about ejection velocities and angles. Finally, a higher resolution (~10 m) DEM of the TVG area would help toward delineating the impact areas more accurately.

Acknowledgements We would like to thank the Ministry Of Science and Technology (MOST) of Taiwan for its support of this research in the form of a Grant awarded to the corresponding author. Aprilia Nurmawati was financially supported by a scholarship awarded by the School of Earth Sciences, National Central University, while studying for her Master's degree. We would also like to thank the Editor-in-Chief V. Schenk for handling the manuscript as well as Daniel Bertin and an anonymous reviewer for their thorough and very constructive reviews.

References

Alatorre-Ibargüengoitia MA, Delgado-Granados H (2006) Experimental determination of drag coefficient for volcanic materials: calibration and application of a model to Popocatépetl volcano (Mexico) ballistic projectiles. Geophys Res Lett 33:L11302. https://doi.org/10.1029/2006GL026195

Alatorre-Ibargüengoitia MA, Scheu B, Dingwell DB, Delgado-Granados H, Taddeucci J (2010) Energy consumption by magmatic fragmentation and pyroclast ejection during Vulcanian eruptions. Earth Planet Sci Lett 291:60–69. https://doi.org/10.1016/j.epsl.2009.12.051

Alatorre-Ibargüengoitia MA, Delgado-Granados H, Dingwell DB (2012) Hazard map for volcanic ballistic impacts at Popocatépetl volcano (Mexico). Bull Volcanol 74:2155–2169. https://doi.org/10.1007/s00445-012-0657-2

Belousov A, Belousova M, Chen C-H, Zellmer GF (2010) Deposits, character and timing of recent eruptions and gravitational collapses in Tatun Volcano Group, northern Taiwan: hazard-related issues. J Volcanol Geotherm Res 191:205–221. https://doi.org/10.1016/jvolgeores.2010.02.001

Bertin D (2017) 3-D ballistic transport of ellipsoidal volcanic projectiles considering horizontal wind velocities and variable shape-dependent drag coefficients. J Geophys Res Solid Earth 122:1126–1151. https://doi.org/10.1002/2016JB013320

Biass S, Falcone J-L, Bonadonna C, Di Traglia F, Pistolesi M, Rosi M, Lestuzzi P (2016) Great balls of fire: a probabilistic approach to quantify the hazard related to ballistics—a case study at La Fossa volcano, Vulcano island, Italy. J Volcanol Geotherm Res 325:1–14. https://doi.org/10.1016/j.volgeores.2016.06.006

Breard ECP, Lube G, Cronin SJ, Fitzgerald R, Kennedy B, Scheu B, Montanaro C, White JDL, Tost M, Procter JN, Moebis A (2014) Using the spatial distribution and lithology of ballistic blocks to interpret eruption sequence and dynamics: August 6 2012 Upper Te Maari eruption, New Zealand. J Volcanol Geotherm Res 286:373–386. https://doi.org/10.1016/j.jvolgeores.2014.03.006

Browne PRL, Lawless JV (2001) Characteristics of hydrothermal eruptions, with examples from New Zealand and elsewhere. Earth Sci Rev 52:299–331

Burgisser A, Arbaret L, Druitt TH, Giachetti T (2011) Pre-explosive conduit conditions of the 1997 vulcanian explosions at Soufriére Hills volcano, Montserrat: II. Overpressure and depth distribution. J Volcanol Geotherm Res 199:193–205. https://doi.org/10.1016/j.jvolgeores.2010.11.14

Cengel YA, Boles MA (2002) Thermodynamics: an engineering approach. McGraw-Hill, Boston

De Michieli Vitturi M, Neri A, Ongaro TE, Lo Savio S, Boschi E (2010) Lagrangian modeling of large volcanic particles: applications to Vulcanian explosions. J Geophys Res 115:B08206. https://doi.org/10.1029/2009JB007111

Fagents SA, Wilson L (1993) Explosive volcanic eruptions–VII. The ranges of pyroclasts ejected in transient volcanic explosions. Geophys J Int 113:359–370

Fitzgerald RH, Tsunematsu K, Kennedy BM, Breard ECP, Lube G, Wilson TM, Jolly AD, Pawson J, Rosenberg MD, Cronin SJ (2014) The application of a calibrated 3D ballistic trajectory model to ballistic hazard assessment at Upper Te Maari. J Volcanol Geotherm Res, Tongariro. https://doi.org/10.1016/j.jvolgeores.2014.04.006

Hairer E, Wanner G (2010) Solving ordinary differential equations II: stiff and differential algebraic problems. Springer, New York

Hoerner SF (1965) Fluid dynamic drag. S. F. Hoerner, New York

Konstantinou KI, Lin C-H, Liang W-T (2007) Seismicity characteristics of a potentially active quaternary volcano: the Tatun Volcano Group, northern Taiwan. J Volcanol Geotherm Res 160:300–318. https://doi.org/10.1016/j.jvolgeores.2006.09.009

Konstantinou KI (2015) Potential for future eruptive activity in Taiwan and vulnerability to volcanic hazards. Nat Hazards 75:2653–2671. https://doi.org/10.1007/s11069-014-1453-4

Lin CH (2016) Evidence for a magma reservoir beneath the Taipei metropolis of Taiwan from both S-wave shadows and P-wave delays. Sci Rep 6:39500. https://doi.org/10.1038/srep39500

Maeno F, Nakada S, Nagai M, Kozono T (2013) Ballistic ejecta and eruption condition of the vulcanian explosion of Shinmoedake volcano, Kyushu, Japan on 1 February 2011. Earth Planets Space 65:609–621. https://doi.org/10.5047/eps.2013.03.004

Mastin LG (1995) Thermodynamics of gas and steam-blast explosions. Bull Volcanol 57:85–98

Mastin LG (2001) A simple calculator of ballistic trajectories for blocks ejected during volcanic eruptions, US Geological Survey, Open-File report, 01-45

Montanaro C, Scheu B, Gudmundsson MT, Vogfjörd K, Reynolds HI, Dürig T, Strehlow K, Rott S, Reuschlé T, Dingwell DB (2016) Multidisciplinary constraints of hydrothermal explosions based on the 2013 Gengissig lake events, Kverkfjöll volcano, Iceland. Earth Planet Sci Lett 434:308–319. https://doi.org/10.1016/j.epsl.2015.11.043

Muffler LJP, White DE, Truesdell AH (1971) Hydrothermal explosion craters in Yellowstone National Park. Bull Geol Soc Am 82:723–740

Nairn IA, Self S (1978) Explosive eruptions and pyroclastic avalanches from Ngauruhoe in February 1975. J Volcanol Geotherm Res 3:39–60

Parfitt EA, Wilson L (2008) Fundamentals of physical volcanology. Blackwell, London, p 230

Rontogianni S, Konstantinou KI, Lin C-H (2012) Multi-parametric investigation of the volcano-hydrothermal system at Tatun Volcano Group, Northern Taiwan. Nat Hazard Earth Syst Sci 12:2259–2270. https://doi.org/10.5194/nhess-12-2259-2012

Sato H, Taniguchi H (1997) Relationship between crater size and ejecta volume of recent magmatic and phreato-magmatic eruptions: implications for energy partitioning. Geophys Res Lett 24:205–208

Song SR, Yang TF, Yeh YH, Tsao SJ, Lo HJ (2000) The Tatun volcano group is active or extinct? J Geol Soc China 43:521–534

Spence RJS, Kelman I, Baxter PJ, Zuccaro G, Petrazuolli S (2005) Residential building and occupant vulnerability to tephra fall. Nat Hazards Earth Syst Sci 5(4):477–494. https://doi.org/10.5194/nhess-5-477-2005

Spieler O, Kennedy B, Kueppers U, Dingwell DB, Scheu B, Taddeucci J (2004) The fragmentation threshold of pyroclastic rocks. Earth Planet Sci Lett 226:139–148. https://doi.org/10.1016/j.epsl.2004.07.016

Taddeucci J, Alatorre-Ibargüengoitia MA, Cruz-Vásques O, Del Bello E, Scarlato P, Ricci T (2017) In-flight dynamics of volcanic ballistic projectiles. Rev Geophys. https://doi.org/10.1002/2017RG000564

Tsunematsu K, Chopard B, Falcone J, Bonadonna C (2014) A numerical model of ballistic transport with collisions in a volcanic setting. Comput Geosci 63:62–69

Wang WH, Chen C-H (1990) The volcanology and fission track age dating of pyroclastic deposits in Tatun Volcano Group. Acta Geol Taiwan 28:1–30

Williams GT, Kennedy BM, Wilson TM, Fitzgerald RH, Tsunematsu K, Teissier A (2017) Buildings vs. ballistics: quantifying the vulnerability of buildings to volcanic ballistic impacts using field studies and pneumatic cannon experiments. J Volcanol Geotherm Res 343:171–180. https://doi.org/10.1016/j.jvolgeores.2017.06.026

Yamagishi H, Feebrey C (1994) Ballistic ejecta from the 1988–1989 andesitic vulcanian eruption of Tokachidake volcano, Japan,—morphological features and genesis. J Volcanol Geotherm Res 59:269–278

Yang TF, Sano Y, Song SR (1999) ^{3} He $/^{4}$ He ratios of fumaroles and bubbling gases of hot springs in Tatun Volcano Group, North Taiwan. Nuovo Cimento C22(34):281286

Zellmer GF, Rubin KH, Miller CA, Shellnutt JG, Belousov A, Belousova M (2015) U-Th isotope constraints on the petrogenetic processes and ages of young effusive eruptions from Tatun Volcano Group, northern Taiwan. In: Carrichi L, Blundy JG (eds) Chemical, physical and temporal evolution of magmatic systems. Geological Society, London, p 175